Environmental Science & Technology

pubs.acs.org/est

Article

Sustaining Irrigation Supplies through Immobilization of Groundwater Arsenic *In Situ*

Jing Sun,[‡‡] Yuqin Sun,[‡‡] Henning Prommer, Benjamin C. Bostick, Qingsong Liu, Meng Ma, Zengyi Li, Songlin Liu, Adam J. Siade, Chao Li, Shuangbao Han, and Yan Zheng*

Cite This: *Environ. Sci. Technol.* 2024, 58, 12653−12663

Read Online

ACCESS | Metrics & More | Article Recommendations | Supporting Information

ABSTRACT: Geogenic arsenic (As) in groundwater is widespread, affecting drinking water and irrigation supplies globally, with food security and safety concerns on the rise. Here, we present push−pull tests that demonstrate field-scale As immobilization through the injection of small amounts of ferrous iron (Fe) and nitrate, two readily available agricultural fertilizers. Such injections into an aquifer with As-rich (200 ± 52 μg/L) reducing groundwater led to the formation of a regenerable As reactive filter in situ, producing 15 m^3 of groundwater meeting the irrigation water quality standard of 50 μg/L. Concurrently, sediment magnetic properties were markedly enhanced around the well screen, pointing to neo-formed magnetite-like minerals. A reactive transport modeling approach was used to quantitatively evaluate the experimental observations and assess potential strategies for larger-scale implementation. The modeling results demonstrate that As removal was primarily achieved by adsorption onto neo-formed minerals and that an increased adsorption site density coincides with the finer-grained textures of the target aquifer. Up-scaled model simulations with 80-fold more Fe-nitrate reactants suggest that enough As-safe water can be produced to irrigate 1000 m^2 of arid land for one season of water-intense rice cultivation at a low cost without causing undue contamination in surface soils that threatens agricultural sustainability.

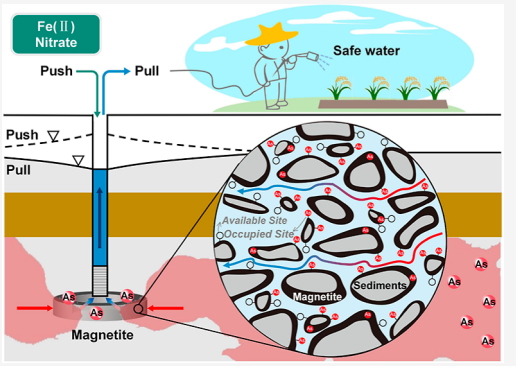

KEYWORDS: *groundwater sustainability, irrigation supplies, arsenic immobilization, field push−pull tests, reactive transport modeling*

1. INTRODUCTION

The Green Revolution greatly increased the productivity of crops and so provided food security for the growing world population.[1] Key to this success was mechanized pumping of groundwater, which provides >40% of the water for irrigated agriculture worldwide.[2] The widespread occurrence of geogenic groundwater arsenic (As), a problem in >70 countries,[3,4] often renders this source water unfit for irrigation. For example, using high-As groundwater for rice cultivation has resulted in As enrichment in surface soils, where it reduces yield and increases As uptake in rice grain.[5−7] Globally, 19.7% of global crop production from 17.2% of irrigated agricultural land (452 billion m^2) on which 42 major crops are grown occurs in As-impacted areas.[8] This not only affects present food security and safety but also increasingly threatens future agricultural production as irrigated surface soils accumulate a large fraction of As from irrigation water over time.[9] Groundwater As mitigation measures are desperately needed to address this expanding agricultural risk, as well as the mortality and morbidity-related health risks of the 94 to 220 million people who rely on domestic well water for drinking and are exposed to unsafe levels of As.[10]

Myriad agronomic practices have been proposed as strategies to minimize the bioavailability of paddy soil As for rice cultivation, with the most effective one being adopting water-saving rice cultivars.[11,12] These approaches largely ignore the source of the problem. Arsenic in groundwater for irrigation is hardly ever directly treated, partially due to the lack of convergence between effectiveness and cost. In situ immobilization, often as the first barrier of a multibarrier treatment train, removes contaminants from the groundwater by adsorption onto or coprecipitation with minerals within aquifer sediments. Immobilizing As by stimulating the (trans)formation of iron (Fe)-based materials has had some success.[13,14] However, the vulnerability of Fe-based materials to become sources of groundwater As with evolving redox conditions and/or changing flow paths has hindered their wide application to remediation efforts in reducing subsurface environments.[15] Precipitation of Fe minerals in thermodynamically stable forms under Fe(III)-reducing conditions common within As-burdened aquifers, for example, magnetite, prevents

Received: April 1, 2024
Revised: June 7, 2024
Accepted: June 12, 2024
Published: June 25, 2024

https://doi.org/10.1021/acs.est.4c03225
Environ. Sci. Technol. 2024, 58, 12653−12663

many of these secondary processes. Under controlled laboratory settings, magnetite formation through the co-injection of Fe(II) and nitrate has been shown to successfully immobilize As in sediments with diverse geochemistry features, even over a prolonged anaerobic period.[16−18] Nevertheless, it is well known that the lab-tested methods would often fail in real heterogeneous aquifers teeming with a wide spectrum of dissolved compounds, minerals, and microbes. It remains unclear whether magnetite forms in situ following Fe(II)-nitrate injection and how domestic and irrigation pumping influences As in the treated groundwater. These answers are critical for evaluating whether As remobilization would occur easily and how much As-safe water could be provided.

Herein, this study uses field push−pull tests conducted in a reducing aquifer with high-As groundwater to establish the viability of this direct treatment method. This study first explicitly tested the effectiveness of the Fe(II)-nitrate approach for As removal under in situ conditions, where (bio)-geochemical and hydrogeological subsurface heterogeneity can pose substantial challenges to efficacy. Constrained by field observations, a process-based numerical model was developed to holistically interpret and quantify the in situ changes induced by Fe(II)-nitrate injection and to further explore the up-scaling potential for larger-scale treatment of irrigation water supplies.

2. MATERIALS AND METHODS

2.1. Field Site and Experimental Wells. The push−pull tests were conducted in an aquifer (38.83°N, 106.35°E) in the rural Yinchuan Basin, China, which is the first of a series of arid and semiarid inland basins along the Yellow River corridor[19,20] (Figure 1A). At this site, the Quaternary sediments in the Yinchuan Basin host a shallow unconfined aquifer with depths between 10 and 40 m and a first deep confined aquifer at depths between 25 and 60 m and 140−160 m.[21,22] Groundwater is a critical water resource for agricultural and domestic supply in the Yinchuan basin, although the resource is compromised by elevated levels of As (Data S1 and Figure S1) resulting from the reductive dissolution of As from sediment Fe(III) oxides.[19,21,22]

A test well YCA5 was newly installed for the experiments of this study, which is ∼25 m away from a set of MLWs installed by the China Geological Survey (Figures 1B and S2). YCA5 reaches a depth of 30 m and uses a 15.9 cm diameter galvanized Fe pipe as casing and a slotted PVC pipe between 22 and 23 m below ground level as screen. The MLWs consist of a bundle of seven PVC pipes to reach the desired depths for each pipe at 3, 10, 23, 30, 40, 50, and 60 mBGL. At the bottom end of each pipe, a 15 cm perforated pipe section acts as a screen.

More details of the site and the well configuration are given in Supporting Information Section S1.1.

2.2. Push−Pull Test Protocol. Two push−pull tests (PPTEST1 and PPTEST2) were conducted in YCA5 to push reagents at the screen depth interval into the surrounding aquifer and to pull groundwater out of the target aquifer after a "storage" period (Figure 1C). Before injection, a PVC pipe with a rubber cap was placed inside YCA5 above the top of the screen to limit the dilution within the casing. Then, native reducing groundwater was sourced from a MLW at 60 m depth at a rate of 1.92 m^3/day using a peristaltic pump (Solinst) and immediately reinjected into YCA5, while care was taken to maintain the reducing condition (Figure 1C). The target depth

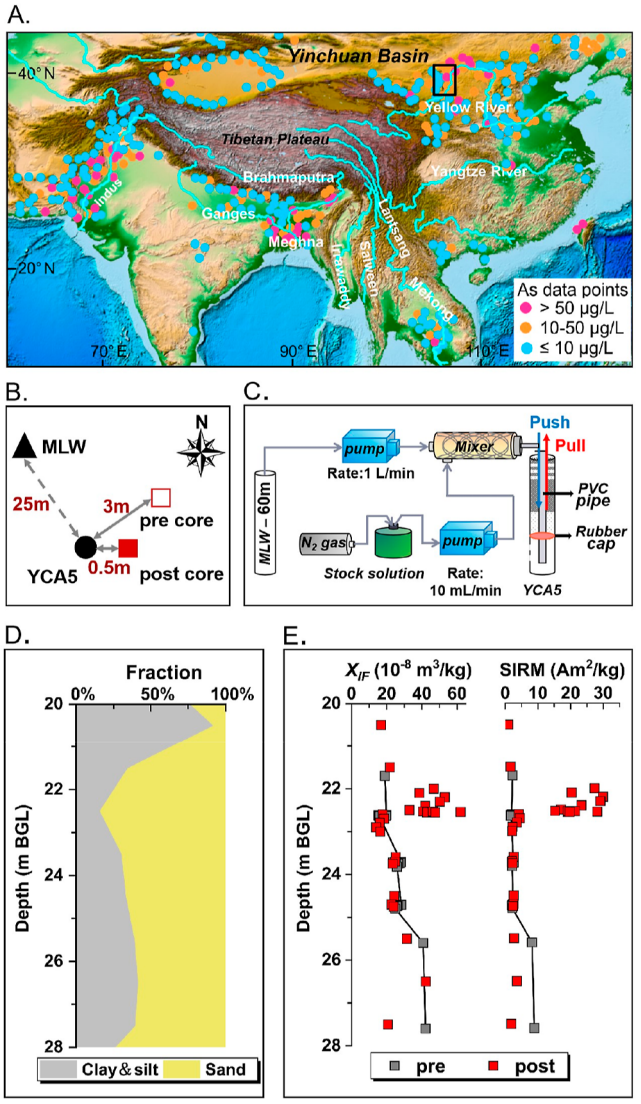

Figure 1. Location of the push−pull test site, experimental design, lithology, and sediment magnetic property. (A) Yinchuan Basin is the first of a series of basins with high-As groundwater along the Yellow River in China. (B) YCA5 with a screen interval at 22−23 mBGL was newly drilled in Sept 2017 for the push−pull tests. Approximately 25 m northwest of YCA5 is a set of multilevel wells (MLWs) with depths of 3, 10, 23, 30, 40, and 60 m. One sediment core (open square) was collected in Sept 2017 for pretest analysis, while another core (filled square) was collected in Dec 2018 for post-test analysis. (C) Conceptual diagram of the injection system used for the tests. Fe(II)-nitrate-amended groundwater from MLW-60 m was injected during the push phase, while residual amendment and treated groundwater were recovered during the pull phase. (D) Lithology based on sediment coring showed the target aquifer at 22−23 mBGL consists of fine sand. (E) Depth profile showed a significant increase of magnetic susceptibility (χ) and saturation isothermal remanent magnetization (SIRM) in post-test sediments (red symbols) compared to pretest sediments (gray symbols) at screen depth. Subplots (A) and (D) were revised from Han et al., (2023).[20]

of the alluvial-fluvial aquifer consists of fine sand (Figure 1D). The source water well MLW-60m and the test well YCA5 are hydrogeologically separated by impermeable clay layers,[19−21] therefore minimizing hydraulic and geochemical interferences during the experiments.

https://doi.org/10.1021/acs.est.4c03225
Environ. Sci. Technol. 2024, 58, 12653−12663

Table 1. Mass of Reactive As, Fe, NO_3, and Conservative Br Tracer Injected and Extracted During Two Push-Pull Tests[a]

test	phase	duration	volume	As removed	As removed	As	Fe	NO_3	Br
		day	m^3	%	$\times 10^{-3}$ mol	$\times 10^{-3}$ mol	mol	mol	mol
PPTEST1	push	4.15	4.2			14.3	6.84	19.64	1.965
	storage	25							
	pull@4 m^3/h	0.3	30.7	69	72.0	32.4	2.46	16.07	2.204
	pull@0.25 m^3/h	0.5	4.8	62	8.7	5.5	0.06	b.d	0.009
	pull@1 m^3/h[b]	15.9[b]	26.1[b]	27[b]	27.8[b]	77.0[b]	0.31[b]	0.02[b]	0.002[b]
	recovery						**41%**	**82%**	**116%**
PPTEST2	push	4.65	5.8			51.1	6.82	18.98	1.901
	storage	82							
	pull@1 m^3/h	58	66.5	53	143.6	102.9	1.70	b.d	1.208
	recovery						**25%**	**0%**	**64%**

[a]Note: "b.d." represents "below the limit of determination", while "-" represents "no determination". [b]The values were calculated based on observation data ending where [As] in the extracted water returned to the ambient level.

During the "push" phase of each test, four cycles of Fe(II)-nitrate amendments were injected (Data S2). Because nitrate travels more rapidly than Fe(II), which sorbs onto aquifer sediments via cation exchange and surface adsorption,[18] Fe(II) and nitrate were injected in an alternating sequence instead of simultaneously (Data S2 and Data S3), thereby stimulating chromatographic mixing and creating a more widely distributed reactive zone. In each cycle, 4 mM Fe(II) (as $FeSO_4 \cdot 7H_2O$) was injected for either 8 or 4 h, and 10 mM nitrate (as $NaNO_3$) and 1 mM inert tracer bromide (as NaBr) were jointly injected for 8 or 4 h subsequent to the Fe(II)-amended injection. The concentrations of the amendments were based on those used in our previous laboratory studies.[16,17] To limit disturbances of the geochemical condition of the groundwater, amendments were added from ×100 concentrated stock solutions by a second peristaltic pump (ISMATEC) through an in-line mixer with a 1:100 ratio into native anaerobic groundwater as it was pumped from the source well MLW-60m into the test well YCA5 (Figure 1C). The stock solutions were purged with high-purity nitrogen and covered with black plastic bags throughout the injection to prevent Fe(II) oxidation due to oxygen and light exposure. A tee valve was installed at the end of the in-line mixer, which allowed the injectant to be sampled and analyzed.

Following a "storage" (no-pumping) period of 25 days for PPTEST1, groundwater was "pulled" from the test well to recover Br and to monitor As removal (Table 1). The pump used in the pull phase had a water meter to record the volume and was the same type as those used by local farmers in irrigation wells. Intermittent pumping and varying rates were used during the pull phase of PPTEST1. The pumping rates were set between 4 and 0.25 m^3/h, which are typical for irrigation and domestic uses (Table 1). The extracted water was regularly sampled and analyzed. The pull phase ended when the concentrations of the monitored species became stable.

About 5 months after the completion of PPTEST1, PPTEST2 was conducted in the same well to assess whether the As removal capacity of the reactive filter could be regenerated. The experimental procedures of PPTEST2 were nearly identical to those of PPTEST1 described above, with the only differences being (i) the storage phase was extended from 25 to 82 days and (ii) a medium pumping rate of 1 m^3/h was used throughout the pull phase, though also only for several hrs per day (Table 1). Unfortunately, in the middle of the storage phase, an unexpected water landscape project (construction of a wetland park) started adjacent to our field site and compromised PPTEST2 (see Google Earth images and digital picture in Figure S2).

More details of the experimental procedure are in Supporting Information Section S1.2.

2.3. Sampling and Analysis. To assess the pretest ambient water quality, groundwater samples were collected from the test well YCA5, the source water well MLWs, and some other nearby wells at the field site. Each well was purged for at least three bore volumes prior to groundwater collection. To monitor the composition of the water injected, 14 and 23 injectant samples were collected from the in-line mixer before reaching YCA5 during the push phases of PPTEST1 and PPTEST2, respectively. Source water from MLW-60 m used for amendment injection and dilution was also periodically collected and analyzed to confirm the water composition stability. To monitor the composition of the water recovered, 227 and 145 groundwater samples were collected from YCA5 during the pull phases of PPTEST1 and PPTEST2, respectively.

Temperature, pH, redox potential, and electrical conductivity of the groundwater were determined on site in a flow cell using a calibrated multiprobe (YSI Proplus; Thermo 501A). Alkalinity was determined on site by Gran titration.[23] Fe(II) and Fe(III) ratios in the Fe-bearing injectant were determined on site by the ferrozine method with a portable spectrophotometer (HACH DR1900).[24] Water samples were filtered with 0.22 μm syringe filters (Whatman) into acid-washed polyethylene bottles and preserved as needed. Arsenate As(V) and arsenite As(III) were separated immediately on site using a cartridge, according to Meng et al. (2001).[25] Water composition was determined by inductively coupled plasma mass spectrometry (Thermo Fisher Scientific Element XR) and ion chromatography (Sunnyvale Dionex ICS-90). For most of our analyzed samples, the major ion charges were balanced within 5%.

Both "pretest" and "post-test" aquifer sediments were also retrieved from the field site for mineralogical characterization. One pretest sediment core was drilled ~3 m away from the test well YCA5 during well installation, while another post-test sediment core was drilled ~0.5 m away from the test well after the completion of PPTEST2 (Figure 1B). Pretest and post-test sediment samples were collected on site at ~1 m depth intervals until 30 mBGL. Additionally, the 1 m screen interval section of the post-test core was sampled on site directly into a 1 m PVC tube and then divided into 10 samples after being

https://doi.org/10.1021/acs.est.4c03225
Environ. Sci. Technol. 2024, 58, 12653−12663

brought back to the laboratory. All of the sediment samples were freeze-dried and powdered using an agate mortar-and-pestle before measurements.

Mass-specific magnetic susceptibility (χ) was measured using a Kappabridge MFK1-FA magnetic susceptibility meter in a magnetic field of 200 A m^{-1} at two operating frequencies, 976 Hz for low-frequency susceptibility (χ_{lf}) and 15616 Hz for high-frequency susceptibility (χ_{hf}). Temperature-dependent susceptibility was also recorded in the range of −200 and 700 °C. IRM was produced with an IM-10−30 pulse magnetizer at a forward field of 1.0 T [SIRM and two reverse fields of −100 mT (IRM_{-100})] and −300 mT (IRM_{-300}). IRM was measured with an AGICOJR-6A spinner magnetometer.

More details of the sample handling and analytical procedures are in Supporting Information Section S1.3.

2.4. Process-Based Numerical Modeling. A process-based model framework was developed to integrate and quantitatively evaluate the experimental observations. Because the unexpected hydraulic disturbances make the modeling of PPTEST2 difficult and unconstrained, only PPTEST1 was analyzed by numerical modeling. First, a local-scale flow model was constructed with MODFLOW[26] to simulate the groundwater flow processes. As the hydraulic gradients were dominated by the injection and extraction fluxes, a one-dimensional, radial-symmetric model[27] was constructed for the simulations (model grid is in Figure S3). The model was radially limited to 20 m. Based on the lithology logs (Figure 1D), the vertical model extent was limited to the injection interval, i.e., the depth zone between 22 and 23 mBGL. The injection and extraction rates were discretized in the model in accordance with the experimental procedure. On the basis of the computed flow field, subsequent solute and reactive transport simulations were performed with PHT3D.[28] The pretest ambient groundwater chemistry data (Data S1) were used to define the initial geochemical conditions, while the data collected from the injectant samples (Data S3) were used to define the injectant composition (Table S1).

The reaction network included four main aspects: (1) the process-based description of the Fe mineral formation induced by Fe(II)-nitrate injection; (2) the simulation of the As coprecipitation with magnetite; (3) a suitable approach to quantify adsorption characteristics and associated surface species, including As; and (4) an exchanger site to account for the evolution of cations and pH buffering capacity of the aquifer. In the following, we provide details for these four aspects of the employed reaction network and describe how the relevant processes were implemented in the model. All other reactions remained consistent with the standard geochemical database WATEQ4F.dat.[29]

Although other Fe minerals might have formed at lower quantities, magnetite was the sole neo-forming mineral that was included in the simulations in this study, which conceptually represented neo-formed Fe oxides more generally. The overall magnetite formation pathway induced by the amendment involves the partial oxidation of excessive Fe(II) by nitrate and the Fe(II)/Fe(III) coprecipitation. The oxidation of dissolved Fe(II) to dissolved Fe(III) by nitrate was modeled as a kinetically controlled process

$$r_{Fe^{2+}\_ox} = k_{Fe^{2+}\_ox} \times C_{Fe^{2+}} \times C_{NO_3^-} \times (A_{OH^-})^2 \quad (1)$$

where $C_{Fe^{2+}}$ and $C_{NO_3^-}$ are the concentrations of Fe(II) and nitrate, respectively, A_{OH^-} is the hydroxyl ion activity, and $k_{Fe^{2+}\_ox}$ is the rate coefficient. The rate expression (eq 1) was originally adopted from previously published modeling studies[30−32] and was consistent with the equation used in our previous model for this Fe(II)-nitrate approach.[18] The employed rate coefficient ($k_{Fe^{2+}\_ox}$) was constrained by the data collected in PPTEST1 (Table S2). Magnetite was allowed to precipitate and/or dissolve (Table S3) following the standard rate formulation derived from transition state theory, where the reaction rate is related to the departure from equilibrium[33]

$$r_{Mgt} = k_{Mgt} \times (1 - SR_{Mgt}) \quad (2)$$

where k_{Mgt} is the rate coefficient, and SR_{Mgt} is the saturation ratio of magnetite, which determines the reaction direction and accounts for the impacts of the dynamically changing geochemical conditions on the reaction rate. The employed thermodynamic constant for magnetite was set consistent with WATEQ4F.dat and was not varied during model calibration. The rate coefficient (k_{Mgt}) was determined as a part of the model calibration process.

Coprecipitation of As with magnetite was simulated by adopting the approach used in our previously published models,[18,34,35] where immobilization rates were stoichiometrically linked with the rates of magnetite precipitation. To be specific, the rate of As coprecipitation was modeled by scaling r_{Mgt} (eq 2) with a static stoichiometry term As_Mgt

$$r_{As\_Mgt} = As\_Mgt \times r_{Mgt} \quad (3)$$

where As_Mgt represents the As molar ratio within magnetite. Such a static As-to-magnetite molar ratio was also used in our previous model for this Fe(II)-nitrate approach,[18] which was based on the relatively constant ratio of As coprecipitation with magnetite determined by sequential extraction in a previous experiment.[17] As_Mgt was calibrated in this study.

The numerical implementation of As adsorption in this study was complicated by (i) the slow physical intragranular diffusion[36−39] and (ii) the spatiotemporally varying geochemical/mineralogical conditions. We therefore invoked the dual-domain mass transfer (DDMT) approach to capture the former, which separates the pore space into a "mobile" and "immobile" domain, and a surface complexation model to capture the latter, which assumes that the finer-grained media, represented by the "immobile" domain, is associated with a higher adsorption site density. Even though the actual adsorption process, i.e., surface complexation, is simulated as an equilibrium reaction, in combination with the DDMT approach, this model creates an "apparent" kinetically controlled adsorption behavior and is therefore suitable to mimic the observed flow-rate dependence of the As breakthrough concentrations during water pumping. In our numerical implementation of this conceptual model, the total number of adsorption sites in both the mobile and immobile domains was stoichiometrically linked with the spatiotemporally varying concentration of the neo-forming magnetite. The model parameters controlling the porosities as well as the site densities in both domains were estimated in the calibration process. The stoichiometries and thermodynamic constants of the protonation and dissociation reactions of magnetite were based on Marmier et al. (1999),[40] which were also used in Dixit and Hering (2003).[41] The stoichiometries and thermodynamic constants of surface complexation reactions of all groundwater constituents on magnetite, such as As,

https://doi.org/10.1021/acs.est.4c03225
Environ. Sci. Technol. 2024, 58, 12653−12663

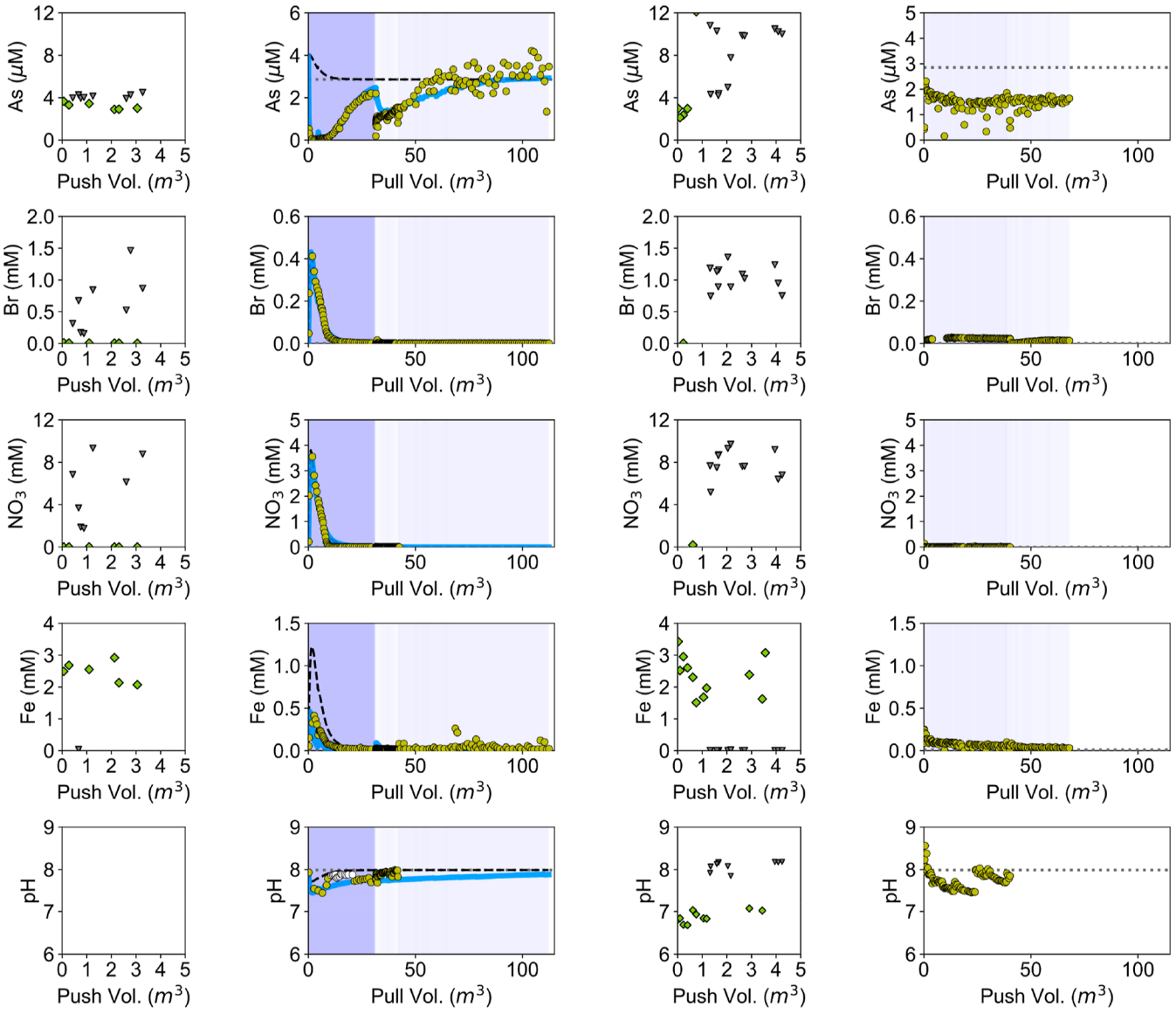

Figure 2. Arsenic, bromide, nitrate, iron, and pH in injected and extracted groundwater versus push or pull volume during two push−pull tests. Left two panels: PPTEST1; right two panels: PPTEST2. The observed groundwater composition is plotted as symbols. Pretest groundwater composition of YCA5 is plotted as gray dotted lines. Final calibrated reactive and conservative transport simulations are plotted as solid blue lines and dashed black lines, respectively. Pumping rates during pull phases vary and are marked by color with light to dark blue indicating increasing rates (darkest blue: 4 m^3/h; lightest blue: 0.25 m^3/h).

sulfate, Fe(II), and Ca, were assumed to be consistent with those on hydrous ferric oxide available in WATEQ4F.dat, which was based on Dzombak and Morel[42] (Table S3). Groundwater phosphate in the target aquifer was nondetected and therefore not considered in the model. The ratio between strong and weak sites was maintained at 1:40, also consistent with Dzombak and Morel.[42] Herein, the As surface complexation reaction on the weak sites was described as

$$\text{Mgt\_wOH} + \text{H}_3\text{AsO}_3 \leftrightarrow \text{Mgt\_wH}_2\text{AsO}_3 + \text{H}_2\text{O} \quad (4)$$

None of the surface complexation constants were varied during the calibration process.

A cation exchanger site (X) was implemented in the model to account for the potential for cation exchange reactions to affect the evolution of the concentrations of cations such as Fe(II), Na, and Ca. Furthermore, although mineral precipitation from Fe(II) oxidation would generate acidity during transport and storage of the injectant, the pH of the recovered water did not significantly decrease. Since no artificial buffer was added in these push−pull tests and no carbonate minerals were found in the sediments in the target aquifer (Figure S4), proton buffering was assumed to be the major pH buffering process.[43,44] The reactions between the proton exchanger site (Y) and the cations (Cat) were simulated by adopting the approach used in our previously published models[43,44]

$$\text{Cat}^{+i} + i\text{Y}^- \leftrightarrow \text{CatY}_i \quad (5)$$

where Cat = H^+, Na^+, K^+, NH_4^+, Ca^{2+}, Mg^{2+}, and Fe^{2+} with proton buffering being one of the cation exchange reactions. The cation (X) and proton (Y) exchange capacities of the native sediments were included in the calibration process, as was the thermodynamic constant for the proton exchange reaction. The thermodynamic constants of the other cation

https://doi.org/10.1021/acs.est.4c03225
Environ. Sci. Technol. 2024, 58, 12653−12663

exchange reactions were kept consistent with WATEQ4F.dat and were not varied during model calibration (Table S3).

A total of 11 parameters were subjected to parameter estimation in this study (Table S2). Following an initial manual trial-and-error calibration, the parameters were further refined by an automatic calibration step such that the sum of the squared residuals between the observations and simulation equivalents was minimized. The automatic calibration was conducted using a heuristic particle swarm optimization (PSO) algorithm due to the significant nonlinearity common in similar models.[45,46] The PSO calibration, which was written within PEST++ and linked with PHT3D, was set with a swarm size of 25, and 400 iterations of the algorithm were conducted. The parameter estimates from PSO were subsequently used as initial values for the Gauss−Levenberg−Marquardt method contained in PEST++ for final calibration refinement as well as parameter uncertainty analysis and sensitivity analysis.[45,46] The observation data used to constrain the automatic calibration consisted of observed pH, As, Br, Fe, nitrate, sulfate, Na, K, Ca, Mg, and Cl concentrations in the recovered water. The procedure of observation weight assignment was adopted from Sun et al. (2018).[18]

More details of the model development, parametrization, and calibration are in Supporting Information Section S2.

2.5. Predictive, Up-Scaled Modeling. To demonstrate the feasibility of the Fe(II)-nitrate remediation strategy for intercepting As during irrigation water use, predictive simulations were conducted to assess the efficiency of an upgraded reactive filter system. Consistent with our model for PPTEST1, a predictive model was also constructed as a single-layer, radial-symmetric model, but the radial extent of the model grid was increased to 100 m to accommodate a larger total injection volume. Ambient (As) was set to 100 μg/L (1.333 μM). The amendment injection sequence and rates were similar to those used in the push−pull tests, except that the concentrations of the amendment were set to 10 times higher. The push phase started on day 0 and lasted for 24, 32, or 40 days, resulting in 60-, 80-, or 100-fold more reactants. The pull phase started on day 100 and lasted for 50 days with continuous extraction at 4 m^3/h. In the predictive simulations, the reaction network and its parametrization were identical with those used in the PPTEST1 simulations. More details of the predictive model setup are in Supporting Information Section S3.

3. RESULTS

3.1. Field Tests Demonstrate Successful Immobilization of Arsenic In Situ. The groundwater chemistry of the target aquifer at 22−23 mBGL is typical of the Yinchuan Basin's Quaternary aquifer,[19] which contains 200 ± 52 μg/L (2.66 ± 0.69 μM) As, generally as arsenite (see 4 year of monitoring data in Data S1). Similarly, the source water used in these tests from 60 mBGL contains 277 ± 30 μg/L (3.69 ± 0.40 μM) As, also mostly as arsenite. For PPTEST1 and PPTEST2, 115.0 and 66.5 m^3 of groundwater were extracted during the pull phase, respectively (Figure 2). The "pulled" groundwater contained demonstrably less As, indicating As immobilization (Figure 2). Total immobilized As amounted to 108.5 mmol for PPTEST1, compared to extracting the same volume of ambient groundwater without treatment (Table 1). PPTEST2 successfully immobilized another 143.6 mmol of As (Table 1). Based on groundwater As speciation analysis,[25] the recovered As was still primarily arsenite in both tests (Datas S4 and S5), indicating the target aquifer remained reducing.

For PPTEST1, groundwater was "pulled" at either high (4 m^3/h), low (0.25 m^3/h), or medium (1 m^3/h) pumping rates (Table 1). Substantial removal of As was achieved for the initial 9 m^3 of extracted water, with [As] remaining below 10 μg/L (0.133 μM) (Figure 2). Then, typical breakthrough behavior for retarded sorbate transport through porous media[47] was observed, with strong retention at first, followed by a steep breakthrough. An abrupt drop of [As] coincided with the lowering of the pumping rate from 4 m^3/h, which is typical of irrigation wells in Yinchuan and elsewhere, to 0.25 m^3/h, a rate mimicking domestic well use. Overall, [As] in the extracted water showed an increasing trend and, in the end, returned to the pretest ambient concentration level, consistent with successive exhaustion of available adsorption sites. The injected Br in PPTEST1 was recovered quickly. Recovery of Br was 74% when the volume of extraction equaled that of the injection, reaching 116% in the end. The residual reactants Fe(II)-nitrate were recovered concomitantly with Br (Figures 2, S5, and S6). Nitrite, a possible product of nitrate reduction, was also monitored but was mostly not detected (Data S4). In total, 41% of Fe and 82% of nitrate were pulled out, suggesting an incomplete reaction, probably either through an incomplete chromatographic mixing of the reactants or because of kinetic controls (Table 1).

Therefore, the "storage" period was extended for PPTEST2, resulting in a complete consumption of nitrate, although 25% of Fe was still recovered (Figure 2 and Table 1). Nitrite was again not detected in PPTEST2 (Data S5). Different from the variable pumping rates used in PPTEST1, a medium pumping rate (1 m^3/h) was used throughout the pull phase in PPTEST2. Unfortunately, the breakthrough behavior of solutes was impacted by hydraulic disturbances from the unexpected construction of a wetland park (Figure S2) adjacent to our field site that started during the storage period and "pulled" reactants and Br tracer toward it. Nevertheless, [As] in the extracted water was relatively stable at ∼100 μg/L (1.333 μM) and therefore below ambient level, with an immobilization of 53% (i.e., 47% recovery) throughout the pull phase (Figure 2). Br recovery was only 4.4% when the volume of extraction equaled that of injection but was 64% at the end of PPTEST2 (Table 1), and it could be higher had the extraction continued. The low [Br] when the second period of extraction resumed after 35 days of hiatus is consistent with a continued migration of injectants away from YCA5 (Figure S5).

To further examine the response of [As] to a sequence of high, low, and medium pumping rates, a "control test" was conducted in YCA5−2.5 years after the completion of PPTEST2, when the reactive filter had exhausted its capacity for As removal. No flow-rate dependence of [As] during water pumping was observed in this test (Data S6). No matter which pumping rate was used, [As] in withdrawals from YCA5 quickly reached the ambient level and remained stable after the bore water was emptied (Figure S7).

3.2. Model Calculation and Magnetic Property Measurement Support Magnetite Formation. A coupled flow, solute, and reactive transport model (RTM)[48] was developed to quantify and deconvolve hydro(bio)geochemical processes induced by Fe(II)-nitrate injection within the aquifer. The model simulations incorporated a multitude of factors, such as time-varying amendment inputs, preferential

https://doi.org/10.1021/acs.est.4c03225
Environ. Sci. Technol. 2024, 58, 12653−12663

flow characteristics, and incomplete hydrogeological mixing, while considering a number of plausible (bio)geochemical reactions. We first simulated the behavior of the amended Br tracer, which allowed us to determine the hypothetical groundwater composition that would have resulted from physical flow and transport alone (black dashed lines, Figures 2, S5 and S6). The similarities between the observations and simulations indicated that during PPTEST1, the concentrations of most monitored species were governed primarily by physical processes. In contrast, the fate of Fe was reaction-driven (Figures 2 and S8). The missing amounts of Fe(II) and nitrate observed (Table 1) are consistent with the amounts of these injected solutes consumed in the reaction in the calibrated model. Differing from our previous study, in which the injected Fe turned into both ferrihydrite and magnetite,[18] it was not possible to measure the concurrent formation of multiple Fe minerals. We thus used magnetite as a proxy for all neo-formed mineral products here. The RTM, in which magnetite precipitation and dissolution were regulated by its thermodynamic stability (with log $K = -3.737$ in WATEQ4F.dat,[29] expressed as $K = [H^+]^8/[Fe^{2+}][Fe^{3+}]^2$, Table S3), suggested that magnetite remained oversaturated within the target aquifer (Figure 3).

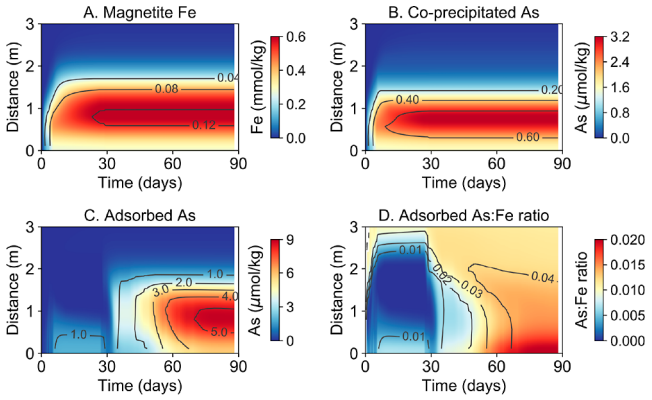

Figure 3. Distribution of neo-formed magnetite and immobilized arsenic as simulated by the RTM for PPTEST1. (A) Simulated Fe in magnetite, (B) coprecipitated As, (C) adsorbed As, and (D) adsorbed As-to-Fe molar ratio are shown. The contour on each subplot represents the concentration or ratio in the transport-limited model domain. The concentration in mol/kg was calculated by assuming a sediment grain density of 2.65 kg/L.

Mineralogical analysis of two sediment cores (Figure 1B), one of which was collected at the time of the test well installation and the other following completion of the push–pull tests, further verified that magnetite was formed from Fe(II)-nitrate injections. Although the mass of neo-formed magnetite appeared to be too low to be quantified using chemical extractions or spectroscopically (Figures 3A and S9) because of the abundant Fe in native sediments,[19,20] neo-formed magnetite was evidently identified within the complex sediment matrix based on the intrinsic and unique magnetic characteristics (Figures 1E and S9). The pre- ($n = 6$) and post-test ($n = 11$) sediment samples surrounding the well screen were compared and contrasted in detail (Table S4). The magnetic susceptibility (χ), sensitive to magnetite and maghemite,[49] increased from $17.2 \pm 1.8 \times 10^{-8}$ to $45.8 \pm 7.1 \times 10^{-8}$ m^3/kg ($p < 0.05$). Temperature-dependent susceptibility measurements of post-test sediment samples further showed that the Verwey transition occurred at about −150 °C, and a sharp drop occurred at about 580 °C, both indicating neo-formed magnetite (Figure S9).[49] In contrast, maghemite lacks a low-temperature transition and has a Curie temperature of 645 °C.[49] SIRM also mirrored the response in χ and increased from 1.9 ± 0.1 to 22.5 ± 4.8 $A \cdot m^2/kg$ ($p < 0.05$). The simultaneous enhancement of χ and SIRM indicates that the grain size of neo-formed magnetite particles remains relatively constant[49] and thus supports increased concentration of magnetite in the push–pull tests impacted aquifer zone.

3.3. Adsorption and Coprecipitation Immobilize Arsenic in a Magnetite-Based Reactive Filter. In laboratory studies, two geochemical processes have been found to be key to As immobilization by magnetite: (i) adsorption onto and (ii) coprecipitation with magnetite.[16−18] This study demonstrates that these mechanisms are also responsible for As immobilization in situ in natural aquifers. Without As coprecipitation, the RTM could not replicate the observed low [As] that occurred in the early part of the pull phase of PPTEST1. The effect of coprecipitation can also be seen in a variant of the calibrated model in which the deactivation of the As coprecipitation process resulted in markedly higher simulated [As] than the observed values (see the calibrated model in Figure 2 versus the model variant in Figure S10). The As/Fe molar ratio in the neo-formed magnetite was estimated to be 1:181 (Table S2), which falls into the previously reported large range for As coprecipitation with magnetite, from 1:2000 via structural substitution[18,50] to 1:4 via surface precipitation.[35,51] Such As coprecipitation, however, was only effective while magnetite was actively forming. Based on our model, it is mostly adsorption on neo-formed magnetite-like minerals that intercepts As advecting toward YCA5 during water extraction (Figure 3). Furthermore, while [As] in water pulled during PPTEST1 always increased toward the ambient concentration as the sorption sites became occupied, [As] suddenly dropped at the onset of the low pumping rate (Figure 2). Such residence time dependence points to rate-limited interactions between the solid phase in the aquifer and the advected groundwater, as elaborated below.

The chemical complexation of As onto (hydr)oxide mineral surfaces typically occurs on the order of milliseconds,[52,53] suggesting a lack of kinetic influence on As retention. Therefore, the (apparent) rate-limited adsorption phenomenon observed in this study is interpreted to be a result of coupled and concomitant hydrogeological-geochemical heterogeneities,[36−39] whereby an increased adsorption site density coincides with the finer-grained textures of the push–pull tests-impacted aquifer zone. In the RTM, this kinetic effect is accounted for using a DDMT process,[43,54] wherein longer residence time due to slower pumping or stop-flow events corresponds to enhanced availability of more abundant but transport-limited surface sites provided by the magnetite-based reactive filter. Based on this conceptual model, our numerical model successfully reproduced the abrupt decrease of recovered water [As] when the pumping rate was lowered by 8-fold (Figure 2). Overall adsorption site density was estimated to be 0.26 mol of sites per mol of magnetite (Table S2), therefore agreeing with its nanoparticulate size.[16,42] Total adsorbed As on magnetite when recovered water [As] returned to ambient level amounted to ∼0.015 mol As per mol Fe (Figure 3D), also falling within the range of 0.008 to 0.023 mol

https://doi.org/10.1021/acs.est.4c03225
Environ. Sci. Technol. 2024, 58, 12653−12663

As per mol Fe based on the typical equilibrium As adsorption isotherm on magnetite.[41]

4. DISCUSSION

4.1. Up-Scaling to Assess the Potential of the Treatment Method. The Fe(II)-nitrate approach was previously shown to be effective in bench-scale experiments with samples from two distinct As-polluted U.S. Superfund sites.[16,17] Here, the in situ experiments in the Yinchuan Basin, China, with naturally occurring As further confirm that immobilization of As through injection of Fe(II)-nitrate amended groundwater is a viable and scalable approach to construct a barrier for human As exposure reduction. Multiple lines of evidence support the formation of magnetite-like minerals in the subsurface, and the associated retention of As. To further illustrate the potential of the Fe-nitrate approach, the RTM, which was developed and constrained by observations from PPTEST1, was subsequently extended to determine As removal in the irrigation water. As an integral part of these predictive simulations, various operational considerations were explored. This process included, for example, the variation in the amount of the Fe(II)-nitrate amendments to increase As sequestration. The simulation results demonstrate that, when the amount of injected amendments is increased to 80-fold of that used in each push−pull test, ∼1300 m^3 of As-safe irrigation water (≤50 μg/L or 0.667 μM As, water quality standard for rice cultivation) can be supplied at a typical high rate of 4 m^3/h (Figure 4). This amount of water is enough for irrigating 1000 m^2 of land for an entire rice cultivation season in the arid Yinchuan Basin,[55] and a larger area if used on less water-intensive crop types or if rainfall is also available. Even where concentrated, the mineral precipitation (Figure 4B) would not occupy more than 0.1% of the available pore space, which implies that the proposed approach would less likely cause pore clogging issues that are often associated with the presence of a zerovalent Fe barrier and its voluminous corrosion products.[56,57]

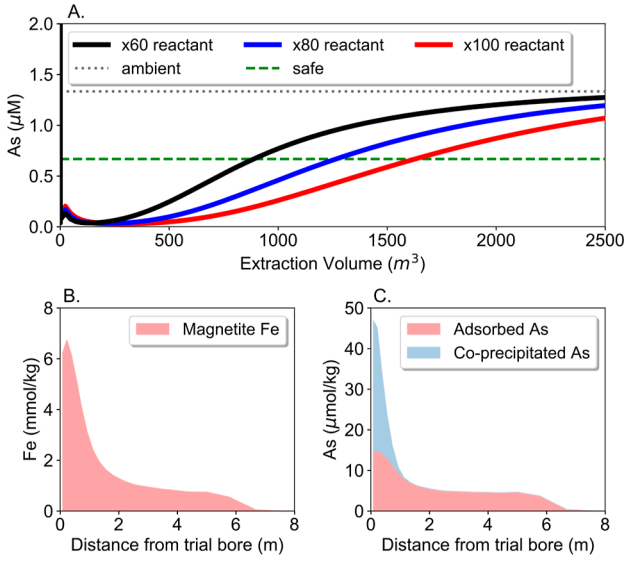

Figure 4. Predictive simulations suggest that an injection with ×80 amount of the iron(II)-nitrate amendment used in each push−pull test could provide enough arsenic-safe water for 1000 $m^2$of land for an entire rice cultivation season in Yinchuan. (A) Simulated [As] in extracted groundwater with 60-, 80-, and 100-fold more reactants are plotted as a solid black line and a solid blue line, respectively. Ambient groundwater [As] used in the simulations (i.e., [As] = 100 μg/L or 1.333 μM) and safe irrigation [As] for rice cultivation (i.e., [As] no more than 50 μg/L or 0.667 μM) are plotted as a gray dashed line and a red dotted line, respectively. Simulated profiles of (B) neo-formed magnetite with 80-fold more reactants and (C) associated coprecipitated and adsorbed As when [As] in extracted water equals safe irrigation [As] for rice cultivation are shown.

This study demonstrates the potential of a limited quantity of magnetite (probably in combination with other Fe minerals) to successfully remediate a reasonably large volume of As-bearing water. Here, the formation of ∼0.05 mol of magnetite yielded 1 m^3 As-safe irrigation water (Figure 4). Further engineering optimization of a push−pull system is necessary for practical applications. Among likely improvements that would further increase the yield of As-safe water are optimized injections that improve the efficiency of in situ mineral formation and optimized withdrawals that maximize the interaction of advected groundwater with the reactive filter. To control the complex effects of hydrogeological-geochemical heterogeneities, subsequent injections should expand on this first attempt using alternate injections of reactants. While beyond the scope of this study, the developed numerical model framework can also be employed to develop a robust engineering design through the rigorous use of predictive simulations for more systematic optimization and uncertainty assessment.

4.2. Implication for Rural Water Safety and Food Security. The treatment method in this study uses two common agricultural fertilizers, Fe and nitrate, to generate a reactive filter for As. The reactive filter, which will remain subsurface, will see a marginal increase in solid-phase As concentration (Figure 3BC). This is because the groundwater contains only a small fraction of the total As in the combined groundwater-sediment system.[19,20] Therefore, the in situ trapping merely represents a slight redistribution of already endowed sediment As without adding any new As. Because magnetite is less susceptible to redox changes under typical aquifer conditions, the stability of the trapped As is also relatively high.[16−18] Fe(II)-nitrate injection is therefore an improvement on the previously proposed treatment technique of nitrate injection for high-As aquifers in Asia,[58,59] which may predominantly produce ferric oxyhydroxides that are vulnerable within reducing aquifers over the long-term. In terms of the injectants, both Fe and nitrate are widely dispersed in the environment. Although nitrate is a contaminant, the risks of injecting nitrate are expected to be manageable. The reasons are 3-fold. First, given that the abstracted volume will always far exceed the injected volume, combined with the fact that groundwater As problem mostly occurs in flat, low-lying areas with sluggish flow,[4] the risk for offsite migration of nitrate is low. Second, while it is conceivable that unreacted nitrate could escape recovery and enter other parts of the aquifer, high-As aquifers are typically anaerobic and thus effectively loci for denitrification. This is evidenced by the absence of measurable nitrate (and nitrite) recovered from PPTEST2 (Figure 2) and in ambient groundwater.[19] Finally, the presence of any residual nitrate in the recovered water represents a tolerable risk, given that nitrate is a nutrient that will benefit crops in irrigation.

Like all water treatments, this Fe(II)-nitrate approach should be accompanied by monitoring to establish whether treatment is effective for As removal. Given that adsorption is the

https://doi.org/10.1021/acs.est.4c03225
Environ. Sci. Technol. 2024, 58, 12653−12663

dominant As removal mechanism, the effectiveness of the reactive filter will be reduced once the amount of As approaches its surface capacity. Nevertheless, the capacity of this reactive filter can be easily "reloaded", as demonstrated by the encouraging results obtained for PPTEST2 (Figure 2). It is worth noting that since the reagents needed for this treatment method are widely available agricultural fertilizers and the equipment is mostly reusable, the direct cost of implementation is estimated at US$ 0.08 per m^3 of treated water (Supporting Information Section S4). For reference, drinking water costs consumers on metered supplies at US$0.50−1.05 per m^3 in Beijing, China[60] and US$1.6 per m^3 in New York City, U.S., in 2024.[61] At this time, only a preliminary cost estimate is possible, and clearly, continued engineering optimization intended for wide adoption by local farmers will likely further reduce the cost estimated here. We therefore conclude that, with continued effort, this Fe(II)-nitrate approach will produce a regenerable, stable reactive filter around the well screen in naturally reducing aquifers to scavenge As at individual irrigation and rural supply wells and, in turn, improve water safety and food security.

■ ASSOCIATED CONTENT

Data Availability Statement

All data needed to evaluate the conclusions in this study are available in the main text and Supporting Information. The relevant software for numeral model development (MODFLOW and PHT3D) and calibration (PEST++), as well as the standard geochemical database (WATEQ4F.dat), are all publicly available. Additional reactions implemented in the database are described in full detail in Supporting Information.

Supporting Information

The Supporting Information is available free of charge at https://pubs.acs.org/doi/10.1021/acs.est.4c03225.

Additional experimental details, materials, methods, figures, and tables (PDF)

Groundwater chemistry of the source well CGS MLW-60m and the target aquifer at 22-23 mBGL; begin and end time, injection and extraction volume and mass of key elements during the push−pull tests; water chemistry of the injectants and residual chemical amendments during push phases of the push−pull tests; water chemistry of extracted water during pull phase of PPTEST1; water chemistry of extracted water during pull phase of PPTEST2; and water chemistry of extracted water in the "control" test (XLSX)

■ AUTHOR INFORMATION

Corresponding Author

Yan Zheng − *Guangdong Provincial Key Laboratory of Soil and Groundwater Pollution Control, School of Environmental Science and Engineering, Southern University of Science and Technology, Shenzhen 518055, China; State Environmental Protection Key Laboratory of Integrated Surface Water-Groundwater Pollution Control, School of Environmental Science and Engineering, Southern University of Science and Technology, Shenzhen 518055, China;* orcid.org/0000-0001-5256-9395; Email: yan.zheng@sustech.edu.cn

Authors

Jing Sun − *State Key Laboratory of Environmental Geochemistry, Institute of Geochemistry, Chinese Academy of Sciences, Guiyang 550081, China; CSIRO Environment, Wembley, Western Australia 6913, Australia; School of Earth Sciences, University of Western Australia, Perth, Western Australia 6009, Australia;* orcid.org/0000-0002-0129-5184

Yuqin Sun − *Guangdong Provincial Key Laboratory of Soil and Groundwater Pollution Control, School of Environmental Science and Engineering, Southern University of Science and Technology, Shenzhen 518055, China; State Environmental Protection Key Laboratory of Integrated Surface Water-Groundwater Pollution Control, School of Environmental Science and Engineering, Southern University of Science and Technology, Shenzhen 518055, China; Key Laboratory of Land Consolidation and Rehabilitation, Land Consolidation and Rehabilitation Center, Ministry of Natural Resources, Beijing 100035, China*

Henning Prommer − *CSIRO Environment, Wembley, Western Australia 6913, Australia; School of Earth Sciences, University of Western Australia, Perth, Western Australia 6009, Australia;* orcid.org/0000-0002-8669-8184

Benjamin C. Bostick − *Lamont-Doherty Earth Observatory, Columbia University, Palisades, New York 10964, United States*

Qingsong Liu − *Department of Ocean Science and Engineering, Southern University of Science and Technology, Shenzhen 518055, China*

Meng Ma − *Guangdong Provincial Key Laboratory of Soil and Groundwater Pollution Control, School of Environmental Science and Engineering, Southern University of Science and Technology, Shenzhen 518055, China; State Environmental Protection Key Laboratory of Integrated Surface Water-Groundwater Pollution Control, School of Environmental Science and Engineering, Southern University of Science and Technology, Shenzhen 518055, China; Department of Irrigation and Drainage, China Institute of Water Resources and Hydropower Research, Beijing 100048, China*

Zengyi Li − *Guangdong Provincial Key Laboratory of Soil and Groundwater Pollution Control, School of Environmental Science and Engineering, Southern University of Science and Technology, Shenzhen 518055, China; State Environmental Protection Key Laboratory of Integrated Surface Water-Groundwater Pollution Control, School of Environmental Science and Engineering, Southern University of Science and Technology, Shenzhen 518055, China*

Songlin Liu − *Guangdong Provincial Key Laboratory of Soil and Groundwater Pollution Control, School of Environmental Science and Engineering, Southern University of Science and Technology, Shenzhen 518055, China; State Environmental Protection Key Laboratory of Integrated Surface Water-Groundwater Pollution Control, School of Environmental Science and Engineering, Southern University of Science and Technology, Shenzhen 518055, China*

Adam J. Siade − *CSIRO Environment, Wembley, Western Australia 6913, Australia; School of Earth Sciences, University of Western Australia, Perth, Western Australia 6009, Australia;* orcid.org/0000-0003-3840-5874

Chao Li − *State Key Laboratory of Environmental Geochemistry, Institute of Geochemistry, Chinese Academy of Sciences, Guiyang 550081, China; College of Earth and Planetary Sciences, University of Chinese Academy of Sciences, Beijing 101408, China*

Shuangbao Han − *Guangdong Provincial Key Laboratory of Soil and Groundwater Pollution Control, School of*

Environmental Science and Engineering, Southern University of Science and Technology, Shenzhen 518055, China; State Environmental Protection Key Laboratory of Integrated Surface Water-Groundwater Pollution Control, School of Environmental Science and Engineering, Southern University of Science and Technology, Shenzhen 518055, China; Center for Hydrogeology and Environmental Geology, China Geological Survey, Baoding 071051, China

Complete contact information is available at: https://pubs.acs.org/10.1021/acs.est.4c03225

Author Contributions

‡‡J.S. and Y.S. contributed equally to this paper. Conceptualization: Y.Z., J.S., H.P., B.C.B.; methodology: Y.Z., J.S., Y.S., H.P., B.C.B., Q.L., A.J.S., C.L.; investigation: J.S., Y.S., M.M., Z.L., S.L., C.L., S.H.; visualization: J.S., Y.S.; funding acquisition: Y.Z., J.S., B.C.B., H.P.; project administration: Y.Z.; supervision: Y.Z., H.P.; writing—original draft: J.S., Y.S., Y.Z.; writing—review and editing: Y.Z., J.S., H.P., B.C.B., Q.L., A.J.S.

Notes

The authors declare no competing financial interest.

■ ACKNOWLEDGMENTS

We would like to thank Tyler Ellis, Baoling Yang, Long Han, and Xuechun Zhang for their assistance. This work was supported by the National Natural Science Foundation of China [41831279, 42321004, and 41772265 to Y.Z., and Excellent Young Scientists Fund Program (Overseas) to J.S.]; the Guangdong Province Bureau of Education [2020KCXTD006 to Y.Z.] and the High-Level University Special Fund [G03050K001 to Y.Z.]; the Chinese Academy of Sciences [Pioneer Hundred Talents Program to J.S.]; the Guizhou "Hundred" High-level Innovative Talent Project [GCC(2023)038 to J.S.]; the U.S. Dept. of Energy [EE0009506 to B.C.B. and H.P.]; the Superfund Research Program of the U.S. National Institute of Environmental Health Sciences [P42ES033719 to B.C.B. and H.P., and P42ES010349 to Y.Z. and B.C.B.]; and the National Science Foundation Signals in the Soil [2226649 to B.C.B.].

■ REFERENCES

(1) Evenson, R. E.; Gollin, D. Assessing the impact of the Green Revolution, 1960 to 2000. *Science* **2003**, *300* (5620), 758−762.
(2) Garduno, H.; Foster, S. Sustainable Groundwater Irrigation. *Approaches to Reconciling Demand with Resources; Strategic Overview Series No. 4 World Bank*: WA, 2010.
(3) Fendorf, S.; Michael, H. A.; van Geen, A. Spatial and temporal variations of groundwater arsenic in South and Southeast Asia. *Science* **2010**, *328* (5982), 1123−1127.
(4) Smedley, P. L.; Kinniburgh, D. G. A review of the source, behaviour and distribution of arsenic in natural waters. *Appl. Geochem.* **2002**, *17* (5), 517−568.
(5) Huhmann, B. L.; Harvey, C. F.; Uddin, A.; Choudhury, I.; Ahmed, K. M.; Duxbury, J. M.; Bostick, B. C.; van Geen, A. Field Study of Rice Yield Diminished by Soil Arsenic in Bangladesh. *Environ. Sci. Technol.* **2017**, *51* (20), 11553−11560.
(6) Dittmar, J.; Voegelin, A.; Maurer, F.; Roberts, L. C.; Hug, S. J.; Saha, G. C.; Ali, M. A.; Badruzzaman, A. B. M.; Kretzschmar, R. Arsenic in Soil and Irrigation Water Affects Arsenic Uptake by Rice: Complementary Insights from Field and Pot Studies. *Environ. Sci. Technol.* **2010**, *44* (23), 8842−8848.
(7) FAO; UNICEF; WHO; WSP. *Towards an Arsenic Safe Environment in Bangladesh*, 2010.
(8) Alam, M. F.; Villholth, K. G.; Podgorski, J. Human arsenic exposure risk via crop consumption and global trade from groundwater-irrigated areas. *Environ. Res. Lett.* **2021**, *16* (12), 124013.
(9) Dittmar, J.; Voegelin, A.; Roberts, L. C.; Hug, S. J.; Saha, G. C.; Ali, M. A.; Badruzzaman, A. B. M.; Kretzschmar, R. Arsenic accumulation in a paddy field in Bangladesh: seasonal dynamics and trends over a three-year monitoring period. *Environ. Sci. Technol.* **2010**, *44* (8), 2925−2931.
(10) Podgorski, J.; Berg, M. Global threat of arsenic in groundwater. *Science* **2020**, *368* (6493), 845−850.
(11) Roberts, L. C.; Hug, S. J.; Dittmar, J.; Voegelin, A.; Saha, G. C.; Ali, M. A.; Badruzzaman, A. B. M.; Kretzschmar, R. J. E. s. Spatial distribution and temporal variability of arsenic in irrigated rice fields in Bangladesh. 1. Irrigation water. *Environ. Sci. Technol.* **2007**, *41* (17), 5960−5966.
(12) Linquist, B. A.; Anders, M. M.; Adviento-Borbe, M. A. A.; Chaney, R. L.; Nalley, L. L.; Da Rosa, E. F.; Van Kessel, C. J. G. c. b. Reducing greenhouse gas emissions, water use, and grain arsenic levels in rice systems. *Global Change Biol.* **2015**, *21* (1), 407−417.
(13) Nikolaidis, N. P.; Dobbs, G. M.; Lackovic, J. A. Arsenic removal by zero-valent iron: field, laboratory and modeling studies. *Water Res.* **2003**, *37* (6), 1417−1425.
(14) Scherer, M. M.; Richter, S.; Valentine, R. L.; Alvarez, P. J. Chemistry and microbiology of permeable reactive barriers for in situ groundwater clean up. *Crit. Rev. Microbiol.* **2000**, *26* (4), 221−264.
(15) United States Environmental Protection Agency. *Arsenic Treatment Technologies for Soil*, 2002. http://www.clu-in.org/download/remed/542r02004/arsenic_report.pdf.
(16) Sun, J.; Chillrud, S. N.; Mailloux, B. J.; Stute, M.; Singh, R.; Dong, H.; Lepre, C. J.; Bostick, B. C. Enhanced and stabilized arsenic retention in microcosms through the microbial oxidation of ferrous iron by nitrate. *Chemosphere* **2016**, *144*, 1106−1115.
(17) Sun, J.; Chillrud, S. N.; Mailloux, B. J.; Bostick, B. C. In Situ Magnetite Formation and Long-Term Arsenic Immobilization under Advective Flow Conditions. *Environ. Sci. Technol.* **2016**, *50* (18), 10162−10171.
(18) Sun, J.; Prommer, H.; Siade, A.; Chillrud, S. N.; Mailloux, B. J.; Bostick, B. C. Model-Based Analysis of Arsenic Immobilization via Iron Mineral Transformation under Advective Flows. *Environ. Sci. Technol.* **2018**, *52* (16), 9243−9253.
(19) Sun, Y.; Sun, J.; Nghiem, A. A.; Bostick, B. C.; Ellis, T.; Han, L.; Li, Z.; Liu, S.; Han, S.; Zhang, M.; et al. Reduction of iron (hydr) oxide-bound arsenate: Evidence from high depth resolution sampling of a reducing aquifer in Yinchuan Plain, China. *J. Hazard. Mater.* **2021**, *406*, 124615.
(20) Han, L.; Sun, Y.; Li, Z.; Duan, Y.; Han, S.; Zhang, H.; Zhao, M.; Zheng, Y. Beyond the geological origin of sediment arsenic in groundwater systems: arsenic redux by redox. *Sci. Bull.* **2023**, *68*, 1616−1620.
(21) Han, S.; Zhang, F.; Zhang, H.; An, Y.; Wang, Y.; Wu, X.; Wang, C. Spatial and temporal patterns of groundwater arsenic in shallow and deep groundwater of Yinchuan Plain, China. *J. Geochem. Explor.* **2013**, *135*, 71−78.
(22) Guo, Q.; Guo, H.; Yang, Y.; Han, S.; Zhang, F. Hydrogeochemical contrasts between low and high arsenic groundwater and its implications for arsenic mobilization in shallow aquifers of the northern Yinchuan Basin, PR China. *J. Hydrol.* **2014**, *518*, 464−476.
(23) Gran, G. Determination of the equivalence point in potentiometric titrations. Part II. *Analyst* **1952**, *77* (920), 661−671.
(24) Horneman, A.; Van Geen, A.; Kent, D. V.; Mathe, P. E.; Zheng, Y.; Dhar, R. K.; O'Connell, S.; Hoque, M. A.; Aziz, Z.; Shamsudduha, M.; Seddique, A. A.; Ahmed, K. M. Decoupling of As and Fe release to Bangladesh groundwater under reducing conditions. Part I: Evidence from sediment profiles. *Geochim. Cosmochim. Acta* **2004**, *68* (17), 3459−3473.
(25) Meng, X.; Korfiatis, G. P.; Christodoulatos, C.; Bang, S. Treatment of arsenic in Bangladesh well water using a household co-precipitation and filtration system. *Water Res.* **2001**, *35* (12), 2805−2810.

(26) Harbaugh, A. W.; Banta, E. R.; Hill, M. C.; McDonald, M. G. *MODFLOW-2000, the US Geological Survey Modular Ground-Water Model: User Guide to Modularization Concepts and the Ground-Water Flow Process*, 2000.
(27) Wallis, I.; Prommer, H.; Post, V.; Vandenbohede, A.; Simmons, C. T. Simulating MODFLOW-Based Reactive Transport Under Radially Symmetric Flow Conditions. *Groundwater* **2013**, *51* (3), 398−413.
(28) Prommer, H.; Barry, D. A.; Zheng, C. MODFLOW/MT3DMS-based reactive multicomponent transport modeling. *Ground Water* **2003**, *41* (2), 247−257.
(29) Ball, J. W.; Nordstrom, D. K. *User's Manual for WATEQ4F, with Revised Thermodynamic Data Base and Test Cases for Calculating Speciation of Major, Trace, and Redox Elements in Natural Waters*, 1991.
(30) Eckert, P.; Appelo, C. Hydrogeochemical modeling of enhanced benzene, toluene, ethylbenzene, xylene (BTEX) remediation with nitrate. *Water Resour. Res.* **2002**, *38* (8), 5-1−5-11.
(31) Wallis, I.; Prommer, H.; Simmons, C. T.; Post, V.; Stuyfzand, P. J. Evaluation of Conceptual and Numerical Models for Arsenic Mobilization and Attenuation during Managed Aquifer Recharge. *Environ. Sci. Technol.* **2010**, *44* (13), 5035−5041.
(32) Zhang, Y.-C.; Prommer, H.; Broers, H. P.; Slomp, C. P.; Greskowiak, J.; Van Der Grift, B.; Van Cappellen, P. Model-based integration and analysis of biogeochemical and isotopic dynamics in a nitrate-polluted pyritic aquifer. *Environ. Sci. Technol.* **2013**, *47* (18), 10415−10422.
(33) Lasaga, A. C. *Kinetic Theory in the Earth Sciences*; Princeton university press, 1998.
(34) Rawson, J.; Prommer, H.; Siade, A.; Carr, J.; Berg, M.; Davis, J. A.; Fendorf, S. Numerical modeling of arsenic mobility during reductive iron-mineral transformations. *Environ. Sci. Technol.* **2016**, *50* (5), 2459−2467.
(35) Rawson, J.; Siade, A.; Sun, J.; Neidhardt, H.; Berg, M.; Prommer, H. Quantifying reactive transport processes governing arsenic mobility after injection of reactive organic carbon into a Bengal Delta aquifer. *Environ. Sci. Technol.* **2017**, *51* (15), 8471−8480.
(36) Darland, J. E.; Inskeep, W. P. Effects of pore water velocity on the transport of arsenate. *Environ. Sci. Technol.* **1997**, *31* (3), 704−709.
(37) Fuller, C. C.; Davis, J. A.; Waychunas, G. A. Surface chemistry of ferrihydrite: Part 2. Kinetics of arsenate adsorption and coprecipitation. *Geochim. Cosmochim. Acta* **1993**, *57* (10), 2271−2282.
(38) Liu, C.; Zachara, J. M.; Qafoku, N. P.; Wang, Z. Scale-dependent desorption of uranium from contaminated subsurface sediments. *Water Resour. Res.* **2008**, *44* (8). .
(39) Dentz, M.; Le Borgne, T.; Englert, A.; Bijeljic, B. Mixing, spreading and reaction in heterogeneous media: A brief review. *J. Contam. Hydrol.* **2011**, *120*−*121*, 1−17.
(40) Marmier, N.; Delisée, A.; Fromage, F. Surface complexation modeling of Yb (III), Ni (II), and Cs (I) sorption on magnetite. *J. Colloid Interface Sci.* **1999**, *211* (1), 54−60.
(41) Dixit, S.; Hering, J. G. Comparison of arsenic(V) and arsenic(III) sorption onto iron oxide minerals: Implications for arsenic mobility. *Environ. Sci. Technol.* **2003**, *37* (18), 4182−4189.
(42) Dzombak, D. A.; Morel, F. M. *Surface Complexation Modeling: Hydrous Ferric Oxide*; John Wiley & Sons, 1990
(43) Sun, J.; Donn, M. J.; Gerber, P.; Higginson, S.; Siade, A. J.; Schafer, D.; Seibert, S.; Prommer, H. Assessing and Managing Large-Scale Geochemical Impacts from Groundwater Replenishment with Highly Treated Reclaimed Wastewater. *Water Resour. Res.* **2020**, *56*, No. e2020WR028066.
(44) Seibert, S.; Atteia, O.; Ursula Salmon, S.; Siade, A.; Douglas, G.; Prommer, H. Identification and quantification of redox and pH buffering processes in a heterogeneous, low carbonate aquifer during managed aquifer recharge. *Water Resour. Res.* **2016**, *52* (5), 4003−4025.
(45) White, J. T.; Hunt, R. J.; Fienen, M. N.; Doherty, J. E. *Approaches to Highly Parameterized Inversion: PEST++ Version 5, a Software Suite for Parameter Estimation, Uncertainty Analysis, Management Optimization and Sensitivity Analysis*; US Geological Survey, 2020.
(46) Siade, A.; Rathi, B.; Prommer, H.; Welter, D.; Doherty, J. Using heuristic multi-objective optimization for quantifying predictive uncertainty associated with groundwater flow and reactive transport models. *J. Hydrol.* **2019**, *577*, 123999.
(47) Selim, H. M. *Transport & Fate of Chemicals in Soils: Principles & Applications*; CRC Press, 2014.
(48) Prommer, H.; Sun, J.; Kocar, B. D. Using Reactive Transport Models to Quantify and Predict Groundwater Quality. *Elements: An International Magazine of Mineralogy, Geochemistry, and Petrology* **2019**, *15* (2), 87−92.
(49) Liu, Q.; Roberts, A. P.; Larrasoana, J. C.; Banerjee, S. K.; Guyodo, Y.; Tauxe, L.; Oldfield, F. Environmental magnetism: principles and applications. *Rev. Geophys.* **2012**, *50*(4). .
(50) Coker, V. S.; Gault, A. G.; Pearce, C. I.; van der Laan, G.; Telling, N. D.; Charnock, J. M.; Polya, D. A.; Lloyd, J. R. XAS and XMCD evidence for species-dependent partitioning of arsenic during microbial reduction of ferrihydrite to magnetite. *Environ. Sci. Technol.* **2006**, *40* (24), 7745−7750.
(51) Wang, Y. H.; Morin, G.; Ona-Nguema, G.; Menguy, N.; Juillot, F.; Aubry, E.; Guyot, F.; Calas, G.; Brown, G. E. Arsenite sorption at the magnetite-water interface during aqueous precipitation of magnetite: EXAFS evidence for a new arsenite surface complex. *Geochim. Cosmochim. Acta* **2008**, *72* (11), 2573−2586.
(52) Sparks, D. L.; Zhang, P. C. Relaxation methods for studying kinetics of soil chemical phenomena. *Rates of Soil Chemical Processes*; John Wiley & Sons, 1991; Vol. *27*, pp 61−94..
(53) Grossl, P. R.; Sparks, D. L. Evaluation of contaminant ion adsorption/desorption on goethite using pressure jump relaxation kinetics. *Geoderma* **1995**, *67* (1−2), 87−101.
(54) Zheng, C.; Wang, P. P. *MT3DMS: A Modular Three-Dimensional Multispecies Transport Model for Simulation of Advection, Dispersion, and Chemical Reactions of Contaminants in Groundwater Systems; Documentation and User's Guide*; DTIC Document, 1999.
(55) Ministry of Ecology and Environment of the People's Republic of China. *Standards for Irrigation Water Quality (GB 5084−2005)*. 2005.
(56) Noubactep, C.; Caré, S.; Crane, R. Nanoscale metallic iron for environmental remediation: prospects and limitations. *Water, Air, Soil Pollut.* **2012**, *223* (3), 1363−1382.
(57) Calabrò, P.; Moraci, N.; Suraci, P. Estimate of the optimum weight ratio in zero-valent iron/pumice granular mixtures used in permeable reactive barriers for the remediation of nickel contaminated groundwater. *J. Hazard. Mater.* **2012**, *207-208*, 111−116.
(58) Omoregie, E. O.; Couture, R.-M.; Van Cappellen, P.; Corkhill, C. L.; Charnock, J. M.; Polya, D. A.; Vaughan, D.; Vanbroekhoven, K.; Lloyd, J. R. Arsenic bioremediation by biogenic iron oxides and sulfides. *Appl. Environ. Microbiol.* **2013**, *79* (14), 4325−4335.
(59) Smith, R. L.; Kent, D. B.; Repert, D. A.; Böhlke, J. Anoxic nitrate reduction coupled with iron oxidation and attenuation of dissolved arsenic and phosphate in a sand and gravel aquifer. *Geochim. Cosmochim. Acta* **2017**, *196*, 102−120.
(60) Water charge in Beijing. 2024. https://www.h2o-china.com/price/view?apid=1&townid=563&ayear=2024 (accessed May 30, 2024).
(61) *New York City Water Board. Water and Wastewater Rate Schedule*. https://www.nyc.gov/assets/nycwaterboard/downloads/pdf/rates/fy2024_rates.pdf, 2024.

https://doi.org/10.1021/acs.est.4c03225
Environ. Sci. Technol. 2024, 58, 12653−12663